Analysis of sampling volume and tissue heterogeneity on the *in vivo* detection of fluorescence

Brian W. Pogue
Dartmouth College
Thayer School of Engineering
Hanover, New Hampshire

Bin Chen
Dartmouth College
Thayer School of Engineering
Hanover, New Hampshire
    and
Dartmouth Medical School
Department of Surgery
Hanover, New Hampshire

Xiaodong Zhou
Dartmouth College
Thayer School of Engineering
Hanover, New Hampshire

P. Jack Hoopes
Dartmouth College
Thayer School of Engineering
Hanover, New Hampshire
    and
Dartmouth Medical School
Department of Surgery
Hanover, New Hampshire

Abstract. The effect of sampling region size and tissue heterogeneity is examined using fluorescence histogram assessment in a rat prostate tumor model with benzoporphyrin derivative fluorophore. Spatial heterogeneity in the fluorescence signal occurs on both macroscopic and microscopic scales. The periphery of the tumor is more fluorescent than the center. Fluorescence is also highest nearest the blood vessels immediately after injection, but over time this fluorescence becomes uniform through the tumor tissue. Using microscopy analysis, the fluorescence intensity histogram distributions follow a normal distribution, yet as the sampling area is increased from the micron scale to the millimeter scale, the variance of the distribution decreases. The mean fluorescence intensity is accurately measured with a millimeter size scale, but this cannot provide accurate measurements of the microscopic variance of drug in tissue. Fiber probe measurements taken *in vivo* are used to confirm that the variance observed is smaller than would be expected with microscopic sampling, but that the average fluorescence can be measured with fibers. Sampling tissue with fibers smaller than the intercapillary spacing could provide a way to estimate the spatial variance more accurately. In summary, sampling fiber size affects the fluorescence intensities detected and use of multiple region microscopic sampling could provide better information about the distribution of values that occur. © *2005 Society of Photo-Optical Instrumentation Engineers.* [DOI: 10.1117/1.2002978]

Keywords: heterogeneity; microscopy; fluorescence; cancer; photodynamic; photosensitizer.

Paper 05062SSR received Mar. 4, 2005; revised manuscript received Apr. 26, 2005; accepted for publication May 6, 2005; published online Aug. 18, 2005.

1 Introduction

Detection of drug concentration *in vivo* has always been a challenging problem in applied biomedical studies. In photodynamic therapy (PDT) or other applications where fluorescence might need to be quantified,[1,2] the method of measuring the fluorescence impacts the magnitude of the signal.[3–5] While in general, careful calibration can be used to interpret the signal and yield a semiquantitative measurement, the problem still remains that different approaches to sampling fluorescence yield vary in results, and cannot easily be compared. Fluorescence within tumors is known to be highly heterogeneous, with a variance that can be as high as 100% of the mean value,[6] and inspection of any fluorescence microscope image will reveal a microscopic-level heterogeneity that changes from near zero to extremely high values.[7–9] In this study, the problem of measuring fluorescence was examined in detail, using flow cytometry, fluorescence microscopy, and *in vivo* measurements with a fiber optic probe that was designed for microsampling of tissues. The interpretation of *in vivo* fluorescence measurements is the key problem, but to fully interpret what these measurements mean, a comprehensive analysis of intensity and variance is required. The distribution of fluorescence intensities observed in tissue is analyzed with a histogram interpretation of the heterogeneity, and this allows comparison between microscopy data and *in vivo* fluorescence data.

One of the major problems in drug quantification is that the sampling volume varies, and the drug is invariably partitioned between different spaces of the tissue, such as vascular, interstitial fluid, extra cellular matrix, and cellular areas. While several studies have been completed comparing *in vivo* fluorescence sampling to dye quantification via tissue extraction methods,[10,11] the results are still confounded by this partitioning issue. In particular, aggregation and microenvironment biophysical changes alter the fluorescence quantum yield,[12–15] and this will cause differences between the *in vivo* fluorescence and the *ex vivo* fluorescence intensities. *Ex vivo* methods typically involve tissue digestion and chemical extraction in a NaOH-type solvent with SDS or some other emulsifying agent.[2,11] This results in a quasimonomeric solution, which should have a maximal fluorescence yield. However, *in vivo* the fluorescence within different compartments of the tissue may have significantly different fluorescence yield values, resulting in a cumulative signal that is not linear

Address all correspondence to Brian Pogue, Thayer School of Engineering, 8000 Cummings Hall, Dartmouth College, Hanover, New Hampshire 03755. Tel: 603–646–3861; Fax: 603–646–3856; E-mail: Brian.W.Pogue@Dartmouth.EDU

with increased drug or not consistently linear over time with the actual drug concentration in the bulk tissue. These changes are quite difficult to prove conclusively, yet perhaps the most important part of this observation is that the fluorescence yield *in vivo* is likely a better reporter of a photophysically active compound.[12,16] There are enough data to support the contention that *in vivo* fluorescence should be used to predict *in vivo* photoactivity.[17,18] Dosimetry based on *in vivo* fluorescence is widely accepted in PDT studies, and methods for advanced interpretation of the *in vivo* signal have been proposed in several recent studies.[19]

This particular work focuses on a more subtle problem than the *ex vivo/in vivo* issue, namely that the size of the sampling volume affects the magnitude and variance of the detected fluorescence signal. In a recent series of studies, the development of an optimized fiber probe was outlined and tested in phantoms and animal tissues.[6,20,21] The design of the probe was developed around the idea that when the sampling volume is smaller in dimension than the average scattering distance in tissue (approximately 100 μm), then the detected fluorescence signal was not highly affected by the tissue optical properties.[20,22] This design was coupled with the idea of using many small sampling fibers, spaced apart by enough distance to minimize cross talk between them. This design proved useful and is now in routine preclinical and human use for PDT dosimetry.[23] However, it is still not obvious that this measured signal is a good representation of the mean and variance of the photosensitizer concentration *in vivo*. Indeed, systematic comparisons between fluorescence microscopy on frozen tissue sections and *in vivo* fluorescence still yield differences in the signal mean and variance.[23] This difference between fluorescence detection methods is the subject examined here, with a particular focus on how well the system measures the spatial variance of the fluorescence *in vivo*. The specific size scales examined here are between 10-μm and 1-mm sampling volume, where the smallest size presents the sampling at a size that is smaller than the typical intercapillary spacing. This distance scale is important, as it presents a primary barrier of drug delivery into tumor parenchyma. Yet sampling of larger volumes is often desired because it can be done macroscopically and feasibly both in preclinical and clinical treatment plans.

In this study, tissues from the same animals are used to compare fluorescence measured *in vivo*, to measurements *ex vivo* on frozen sections using microscopy. The histogram distribution of values are examined and compared. Finally, the partitioning between vascular and stromal spaces is quantitatively analyzed with image processing software, to examine how the transition from vascular localization to stromal localization affects the measurements. This was completed with the clinically used drug verteporfin for injection, which is a lipid formulation of the photosensitizer molecule benzoporphyrin derivative. The photophysical activity of such a mixture is complex, making an interpretation of the sampling volume and microenvironmental effects even more important for accurate dosimetry measurements.
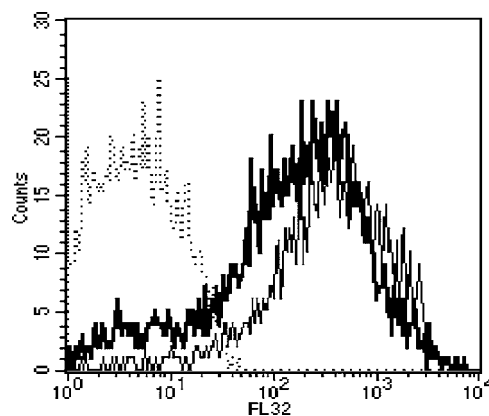
Fig. 1 Flow cytometry histograms showing cellular uptake of verteporfin *in vivo,* assayed *ex vivo* after the tumor cells were removed and disaggregated. Control (dotted line); 15 min after verteporfin injection (thick line); 3 h after verteporfin injection (thin line).

## 2 Materials and Methods

2.1 *Photosensitizer*

The photosensitizer verteporfin was used in this study, which is a lipid formulation of benzoporphyrin derivative (BPD).[13,24,25] This was obtained from QLT Incorporated (Vancouver, Canada). A stock saline solution of verteporfin was reconstituted according to the manufacturer's instructions and stored at 4 °C in a covered tube. This stock solution was injected intravenously to animals at various times prior to use, with a dose of 1.0 mg/kg. The time points of 15 min, 3 h, and 6 h were analyzed for most studies to examine the fluorescence as a function of time after injection. The fluorescent molecule is referred to as BPD in this study, whereas the injected agent is commonly called verteporfin, which includes the BPD and the lipid carrier with solution.

2.2 *Tumor and Animal Models*

The R3327-MatLyLu Dunning prostate tumor model was used in this study, which is an androgen-independent carcinoma, syngeneic to the Copenhagen rat. These R3327-MatLyLu prostate cancer cells were obtained from Tayyaba Hasan's laboratory, and were cultured in RPMI-1640 with glutamine (Mediatech, Herndon, Virginia) supplemented with 10% fetal bovine serum (HyClone, Logan Utah) and 100 units/ml penicillin-streptomycin (Mediatech).

All animal procedures were carried out according to a protocol approved by the Dartmouth College Institutional Animal Care and Use Committee (IACUC). Copenhagen rats (male, 6 to 8 weeks old) were used in this study, and were obtained from Charles River Laboratories (Wilmington, Massachusetts).

Subcutaneous MatLyLu tumors were induced by injecting approximately 1×10^5 MatLyLu cells (suspended in 0.05-ml PBS) subcutaneously into the animal flank after shaving. The tumor growth was measured daily with calipers. Tumors were used for the experiment at 9 to 12 days after inoculation, with a surface diameter of 7 to 9 mm and a thickness of 2 to 4 mm.
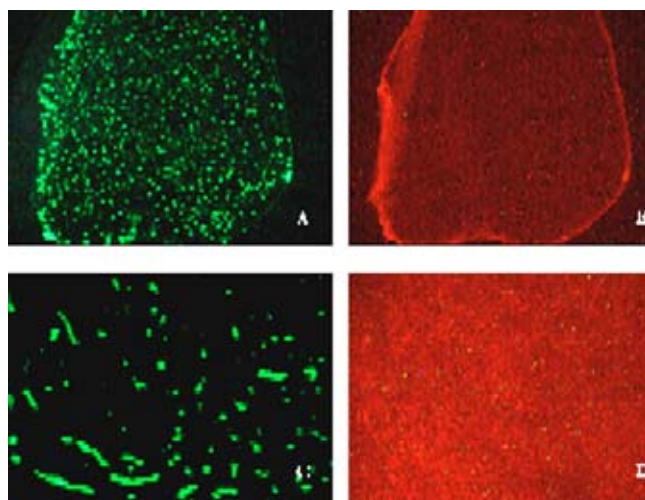
Fig. 2 Images of vascular marker DiOC7 [left, (a) and (c)] and BPD fluorescence [right, (b) and (d)] at different magnification views of the same tumor type, including $4\times$ on the top row [(a) and (b)] and $40\times$ on the bottom row [(c) and (d)]. These images were acquired 3 h after verteporfin injection, and illustrate the macroscopic variation that exists from (b) the edge to the center of the tumor, which is not reflected in (a) the vascular pattern.

2.3 Flow Cytometry

Tumor tissues were excised at 15 min and 3 h after injection of verteporfin (1 mg/kg, i.v.) and minced under sterile and subdued light condition. The minced tumor tissue was digested in sterile PBS containing 0.05% protease (Sigma type 9), 0.02% DNase (Sigma type 1), and 0.02% collagenase (Sigma type 4) under continuous shaking at 37 °C for 40 min, as described previously.[26] The resultant single cell suspension was passed through a cell strainer (BD Biosciences) to remove any remaining tissue clumps and cell aggregates. Verteporfin fluorescence intensity was analyzed by a FACScan (BD Biosciences). 10,000 cells were captured from each sample and verteporfin signal was read in FL32 channel (488-nm excitation and 610-nm long-pass emission) using a log amplifier.

2.4 Fluorescence Microscopy

The fluorescence of verteporfin was analyzed by fluorescence microscopy of the frozen tumor sections, at time points of 15 min, 3 h, and 6 h following drug injection. To visualize the perfused blood vessels, a carbocyanine dye perfusion marker DiOC7(3) (Molecular Probes, Eugene, Oregon) was also injected intravenously at a dose of 1 mg/kg one minute before excising the tumor tissue. Tumors were surgically removed from the animal immediately after sacrifice, and the tumors were embedded in TissueTek medium and snap-frozen immediately in liquid-nitrogen-cooled isopentane. Cryosections of 10 μm thickness were cut from the frozen tumor and the same microscopic fields were imaged for both verteporfin (excitation 425/40 nm, emission 700/30 nm) and the perfusion marker DiOC7(3) (excitation 480/20 nm, emission 540/40 nm) with a Nikon Diaphot-TMD fluorescence microscope.
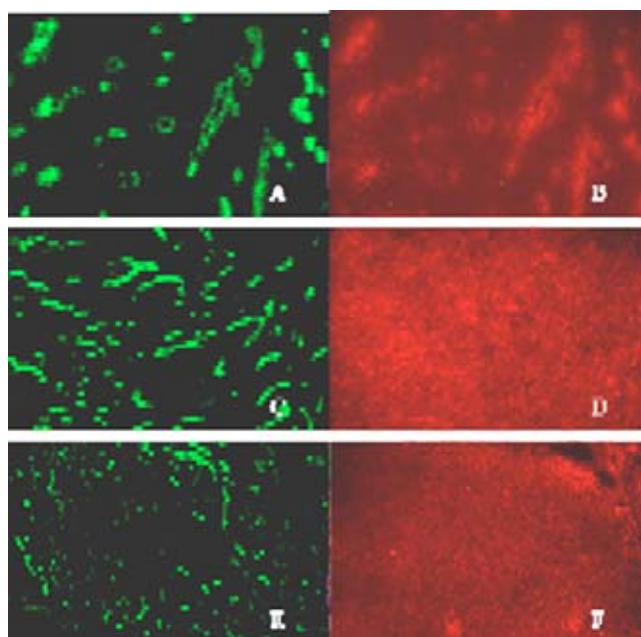
Fig. 3 Images of (a), (c), and (e) vascular perfusion marker $DiOC_7$ and (b), (d), and (f) BPD fluorescence and are shown superimposed together from frozen tissue slices of tumor. The three images show representative distributions where the tumor tissue was resected and frozen at different times after BPD injection, including (a) 15 min, (b) 3 h, and (c) 6 h. The $DiOC_7$ was injected within 5 min before the tumor resection in all cases.

2.5 In Vivo Fluorescence Quantification

In vivo measurements were taken with a specially designed fluorimeter fiber-based system that microsamples the tissue volume.[20,21,23,27] The probe end was designed with 100-μm-diam fibers to constrain the volume of tissue sampled to be smaller than the average scattering distance of tissue (typically 100 to 200 μm).[20] The system has been tested in several phantoms and animal studies, and has been systematically compared to tissue extraction values, using the photosensitizer tetrasulphonated aluminum phthalocyanine.[21] In this study, the system was used to monitor fluorescence at multiple sites on the surface of the tumor, using 20 distinct locations and sampling 10 times from each site. The system was designed to sample each location for 0.5 s and leave less than 1% bleached from each spot for each measurement. In practice, the repeated measurements from each location were analyzed to determine that photobleaching had not caused a significant systematic decrease in the values during the 10 repeated measurements. The set of 200 data points for each animal was used to generate a histogram of fluorescence intensities for each animal. The histograms of individual animals were then cumulatively analyzed to create an average histogram for animals injected 15 min prior to measurements, and animals injected 3 h prior to measurements.

2.6 Image and Statistical Analyses

Image analysis was completed on several microscopic fields from each section of the tumors. The intensity of the fluorescence in each pixel and in each image was assessed with custom written MATLAB programs[28] to quantify the fluores-
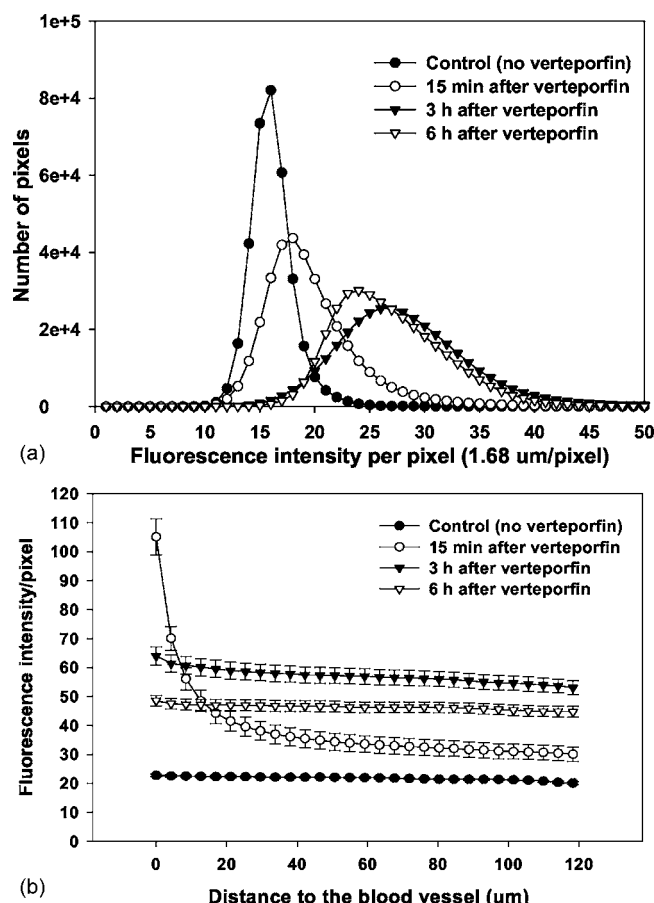
(a)

(b)

Fig. 4 Fluorescence in tumor tissue as quantified by microscopy analysis is shown in (a) as histograms showing the distribution of fluorescence intensity and (b) as a function of distance from the capillaries. Analysis was completed on about 40 frozen sections images from three animals in each group.

cence as a function of distance from the capillary wall in the tumor tissue. Paired images of capillaries, stained with DiOC7, and images of BPD fluorescence were used for the analysis, and the average intensity per pixel was quantified for each distance from the vessel wall (software can be run online or downloaded from http://biolight.thayer.dartmouth.edu). Assessment was completed for histogram-based analysis of the data, as well as analysis of fluorescence as a function of distance from the capillaries.

The analysis of histogram mean and variance values was completed with standard student t- and f-test statistics. For differences in the mean of two distributions, the unpaired t-test provided the p-values for these. For comparisons where the variance was thought to change due to sampling volume changes, the f-test statistic was used, which is defined as the ratio of the variances. Using all the raw data, a p-value is calculated for the hypothesis that the two distributions have equal variance values, with a low p-value indicating that the variances are not equal. Thus a low p-value indicates that the distribution shapes are significantly different, even if the mean values are found to be the same.
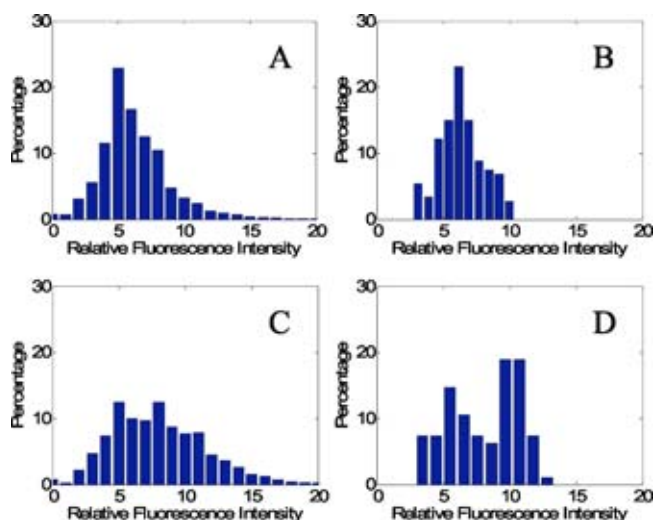

Fig. 5 Histograms of fluorescence intensity are shown for analysis from frozen section microscopy data, as listed in the previous figure, with the tissue resected 15 min after verteporfin injection (top row) and 3 h after injection (bottom row). The two sets of graphs show the analysis completed where each pixel was taken separately and all pixels in all images were used (left column graphs). Also, the data are reported (in the right column) where the entire image fluorescence intensities were used, such that each histogram represents a higher spatial averaging. The data are taken from six to seven animals in each group, using three slice sections for each tumor, and 147 and 95 images total, for the 15-min and 3-h data, respectively. For the pixel data, all pixels in the image were used, corresponding to 349,133 values per image. Analysis of the histogram differences and similarities is quantified in Table 1.

3 Results

3.1 *Flow Cytometry Analysis of Cellular Fluorescence*

Histogram data from the cell flow cytometry experiments are shown in Fig. 1. The data include three groups of cells: 1. control tumor cells having no verteporfin *in vivo*, 2. tumor cells extracted 15 min after verteporfin injection *in vivo*, and 3. tumor cells extracted 3 h after verteporfin injection *in vivo*. Animals were used with injection at the same concentration of 1 mg/kg of verteporfin. The flow cytometry results show histograms of fluorescence intensity (*x* axis) versus number of cells (*y* axis). This distribution of fluorescence values is routinely displayed on a logarithmic scale in flow cytometry analysis, as the signal was amplified in this manner, thus the resulting graph is shown in a linear representation of the signal intensity. Representative flow cytometry histograms are shown in Fig. 1. The width of each histogram indicates that a large variation exists in the amount of photosensitizer per cell. The mean fluorescence intensity of the control sample is 7.4 and the mean intensity values increase to 342.6 and 611.4 at 15 min and 3 h after injection, respectively ($p < 0.01$). This experiment was repeated three times and they all showed the same trend. The potential wash out of BPD from the cells during the processing is a potential artifact of the procedure, but one that cannot be readily solved in this type of assay.

3.2 *Fluorescence Microscopy of Frozen Tumor Sections*

To quantify verteporfin fluorescence intensity in the tumors, several approaches were taken in interpretation of the images.

Table 1 Data are reported for the histograms shown in Figs. 5(a) and 5(b) for 15 minute data, and in Figs. 5(c) and 5(d) for 3-h data. The mean ($\langle f \rangle$) and standard deviation (σ) for each histogram is shown in the third column. The fourth column reports on the p-value that the means of the pixel and image values are different (i.e., $\langle f_I \rangle \neq \langle f_p \rangle$), with the results showing that the two 15-min histograms are significantly the same, and the two 3-h histograms are as well, in terms of their mean values. In the fifth column, the results of the f-statistic are shown, which are the ratio of the variances. In the sixth column, the f-test p-values are shown for the hypothesis that the variances are equal (i.e., $\sigma_I^2 = \sigma_p^2$), showing that the probability is zero that these variances at the pixel and image levels are equal.

Histogram	Number of samples	Mean ± standard deviation ($\langle f \rangle \pm \sigma$)	Mean value t-test p-value for $\langle f_I \rangle \neq \langle f_p \rangle$	f-test statistic σ_I^2 / σ_p^2	Variance value f-test p-value for $\sigma_I^2 = \sigma_p^2$
15-min pixel	5.1×10^7	6.4±3.2	0.008	0.29	0.000
15-min image	147	6.4±1.7			
3-h pixel	3.3×10^7	8.1±3.9	0.009	0.50	0.000
3-h image	95	8.1±2.7			

For each tumor, several magnifications were used for sampling the tumor. The images shown in Fig. 2 illustrate one aspect of the BPD distribution observed in these tumors, which is that the fluorescence intensity observed is significantly higher in the periphery of the tumor as compared to the center. This is a common observation of some experimental tumors, yet in any given field at higher magnification [Fig. 2(d)], the BPD distribution can appear quite homogeneous. These images were taken from tissue removed 3 h after BPD injection. Interestingly, the BPD fluorescence pattern in Fig. 2(b) is not representative of the perfused vascular pattern shown in Fig. 2(a), but the periphery of the image is on average two times as high in fluorescence as compared to the center of the image. This estimate of a factor of 2 is a bulk average value, estimated by quantifying the fluorescence in ImageJ software taking the average over the exterior 100-μm periphery to the interior volume inside this 100-μm ring around the tumor rim.

In addition to this observation, many sample images were taken at 40× magnification to analyze the fluorescence per pixel across average regions of the tumor. Representative images are shown in Fig. 3, with the perfused blood vessels areas shown by DiOC7 fluorescence [Figs. 3(a), 3(c), and 3(e)], and the second set of fluorescence images (right column) being BPD. Images were taken at 15-min, 3-h, and 6-h postinjection. Control images with no verteporfin injected were also taken and had very low levels of fluorescence intensity in the BPD images, as is reported in the next figure. All animals were injected with 1 mg/kg of BPD in verteporfin.

These types of images were acquired from three to five animals in each time point, and three sections were taken from each tumor. Within each section, up to 12 microscopic fields were randomly sampled. The fluorescence per pixel histograms were calculated for the different time points, using frozen tumor sections from multiple animals, to quantify average cumulative histograms of the fluorescence at 15 min, 3 h, and 6 h after injection of verteporfin. These histograms are shown in Fig. 4(a). Because small amounts of fluorescence are present in uninjected animals with tumors as well,

due to autofluorescence and leakage through the filters, the same analysis was completed in uninjected control tumors. In general, the uninjected animal tissues had low fluorescence on this setting (mean near 15 arbitrary units), the 15-min time point showed higher fluorescence (mean near 19 arbitrary units), and the 3-h and 6-h data had respectively higher mean values (near 27 and 29 arbitrary units, respectively). This analysis was completed without subtracting the background fluorescence from the sample data, whereas in the data presented in the next figure (Fig. 5), all histograms have more data included, and have a background subtraction.

The spatial heterogeneity in these images was analyzed using a MATLAB program, which found the vessel locations and then binned intensity values radially outward from the vessel walls. The values summed from multiple images are reported in Fig. 4(b), showing the control, 15-min, 3-h, and 6-h tissue data. The higher concentration near the vessel wall at 15 min illustrates the diffusion gradient of drug coming out from the vessel at this early time, whereas the longer time points of 3 and 6 h show comparatively flatter distributions, indicating there was no strong gradient.

3.3 *Histogram Analysis of Fluorescence Microscopy*

The histogram data from fluorescence microscopy were analyzed in two ways. Since multiple animals and multiple sections were used, there is sufficient data to quantify the fluorescence on different spatial scales. The fluorescence intensity per pixel was quantified for each image, and these were summed into a single histogram, reported in Figs. 5(a) and 5(c), for the 15-min and 3-h time points, respectively. Next, the fluorescence intensity per image was quantified as well, providing a fluorescence intensity measure that averages a considerably larger volume of tissue (1 mm square), rather than for each pixel in the images. This latter approach was used to create histograms as well, and these are shown in Figs. 5(b) and 5(d). While the data in these two sets of graphs are derived from the same images, the resulting histograms have differences from each other, notably that the variance is
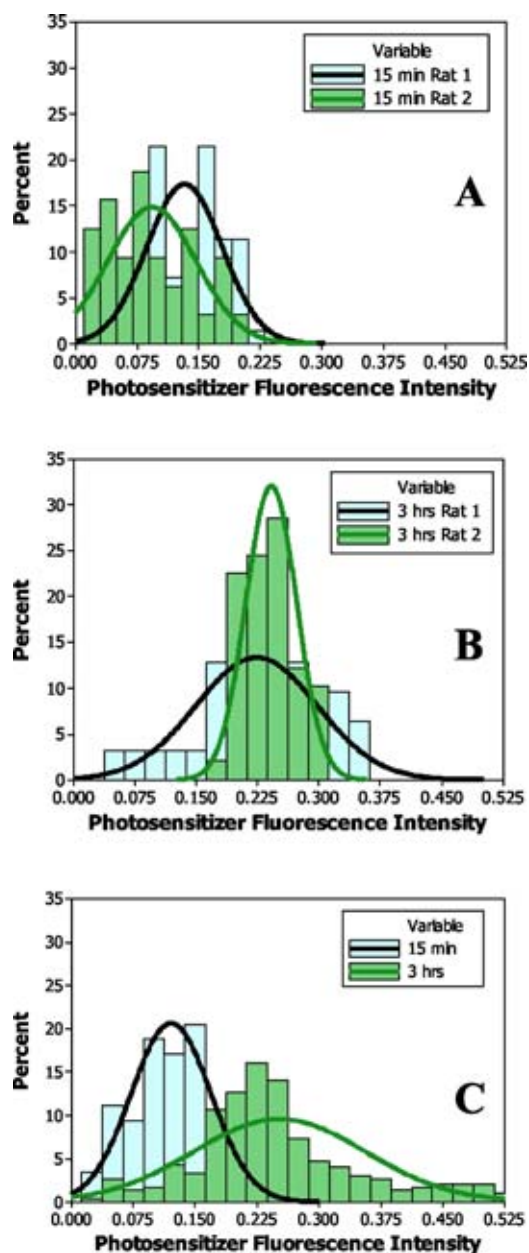
Fig. 6 Histogram data for *in vivo* fluorescence microsampling of tissue is shown here, with two individual animal data sets shown in (a) and (b) for 15-min and 3-h time points, having between 31 and 70 separate data points for each animal. The fitted normal distribution curves are superimposed on top of the data. In (c), the average values from four and five animals, respectively, are shown to illustrate a cumulative dataset for each time point. Mean and variance values for these three histograms along with the analysis are shown in Table 2.

reduced in the latter cases Figs. 5(b) and 5(d), as compared to Figs. 5(a) and 5(c).

The data were fit to a normal distribution, and clearly the datasets in Figs. 5(a) and 5(c) are more optimal for this, as they have larger numbers of data. The mean values and variance of each distribution can be calculated for the distributions in Figs. 5(b) and 5(d), which are analogous to the *in vivo* measurements reported in the next section. As stated in the previous section (discussing Fig. 4), the histograms in Fig. 5

include a larger number of samples and have background subtracted values reported, to exclude the signal due to the background fluorescence.

For the 15-min data, the mean is 6.4 for both pixel and image level sampling, and yet the variance was 1.7 for image level sampling and 3.2 for pixel level sampling. This difference in the variance is statistically different, as shown by the f-test statistic in Table 1, where the probability that the variances are equal is determined to be 0.000. For the 3-h data, the mean is 8.1 for both the pixel and image level sampling of the fluorescence, and yet the variance was 2.7 for image level sampling and 3.9 for pixel level sampling. Again, this is significantly different (Table 1), indicating that the distributions are fluorescence are different based on the size scale of sampling.

3.4 *In Vivo Fluorescence Measurements*

In vivo measurements of BPD fluorescence were taken using several animals as discussed in the materials section. The histogram of fluorescence intensities for two individual animals can be seen in Figs. 6(a) and 6(b), for the cases of 15-min and 3-h postinjection of verteporfin. These individual data are shown to illustrate how each animal typically has a smaller variance in the data distribution, as compared to the overall variance observed in the data summarized for five animals, shown in Fig. 6(c). Even though 100 data points were acquired from each tumor, as shown in Figs. 6(a) and 6(b), the histograms do not show many high and low values, as compared to the cumulative graph in Fig. 6(c).

In Fig. 6(a), the mean and variance values are tabulated in Table 2 as 0.13 and 0.05 for rat 1, and 0.09 and 0.05 for rat 2. These two distributions have a similar variance, but different mean values. These two samples are simply illustrative of an overall trend that is seen from sampling many different animals, which is that the variance of the distribution is often the same, but the mean value between animals can be different. In Fig. 6(b) the mean and variance values are tablulated in Table 2 as well, and are 0.22 and 0.07 for rat 1, and 0.24 and 0.03 for rat 2. In this case, the drug has distributed more homogeneously in the tissue, the mean values are much closer between animals, and the variance of the distribution is seen to be different. In Fig. 6(c), when the composite data are plotted for both the 15-min and 3-h time points using several animals, the mean and variance values are listed in Table 2, and are 0.12 and 0.05 for 15 min, and 0.25 and 0.10 for 3 h. These two distributions have different mean values and different variances, where both the mean and the variance increase by a factor of 2 between the 15-min and 3-h time points.

4 Discussion

While a large number of research studies use fluorescence measurements from tissue as a tool to assess concentration or relative changes in concentration of photosensitizes, comparably little has been published on the effect of how the measurements are done. In the past two decades or so, knowledge of how the tissue scattering affects the detected signal has significantly improved, to the point where it is possible to simulate and predict measured signals, given predictions of the bulk tissue optical properties. However, in all these stud-

Table 2 Data are reported for the histograms shown in Fig. 6 for the two sample rats shown in Fig. 6(a) for 15-min data, Fig. 6(b) for 3-h data, and Fig. 6(c) for summary data. The mean and standard deviation for each histogram is shown in the third column. The fourth column reports on the p-value that the means are the same, with the results showing that the two 15-min histograms are significantly different, and the two 3-h histograms are as well, in terms of their mean values. In the fifth and sixth columns, the results of the f-statistic are shown, where the variance is significantly lower in the image histogram for the 3-h case, but not the 15-min case. When comparing the 15-min data to the 3-h data, the variance is also significantly different.

Histogram	Number of samples	Mean ± standard deviation ($\langle f \rangle \pm \sigma$)	Mean value t-test p-value for $\langle f_1 \rangle = \langle f_2 \rangle$	f-test statistic σ_1^2 / σ_2^2	Variance value f-test p-value for $\sigma_1^2 = \sigma_2^2$
Rat 1, 15 min	70	0.13±0.05	0.008	0.73	0.283
Rat 2, 15 min	32	0.09±0.05			
Rat 1, 3 h	31	0.22±0.07	0.009	0.17	0.000
Rat 2, 3 h	49	0.24±0.03			
Summary 15 min	117	0.12±0.05	0.000	0.21	0.000
Summary 3 h	300	0.25±0.10			

ies, both simulations and experimental, the microregional fluctuations in optical properties and the microregional changes in drug compartmentalization are largely ignored. This is a practical issue, as compensating or accommodating these changes is exceptionally difficult. However, in this study the focus has been on understanding these changes spatially and temporally, to allow a full understanding of the limitations of our measured signal.

When the photosensitizer is injected in the animal and is distributed by the vascular tree, the diffusion of the drug occurs into the tissue, and there are two levels of heterogeneity that are observed. First, there is considerable macroscopic heterogeneity, which is induced by the physical features of the tumor, as shown in Fig. 2(b), where the concentration in the peripheral regions of the mass are on average about two times as high as in the center of the image. This large degree of macroscopic spatial heterogeneity is clearly problematic, yet well documented in both chemotherapy and photodynamic therapy drug distribution studies. The origins of macroscopic spatial heterogeneities are still not well understood, even after considerable research, yet are largely attributed to pressure gradients slowing the diffusive process.[29] This is a static phenomenon that needs to be understood and used when interpreting measurements from the surface of tumors. The current fiber optic design used here[20,21,23,27] was designed specifically to sample shallow regions of tissue because of the need for reducing the effect of tissue light scattering on the measured signal. The design works well for what it is proposed for, but will ultimately only sample the most superficial 200 to 300 μm of tissue, which is the region where the drug concentration is highest. Thus, this design of a fiber probe is not ideal for the tumor type where the periphery of the tumor is so substantially higher than the interior. An interstitial fiber probe or a macroscopic diffuse sampling probe would be required to measure from the interior of the tumor. This is a static problem in drug sampling from tissue, which can confound many studies of drug delivery *in vivo*.

The origin of the spatial heterogeneity observed in Fig. 3(b) at the 15-min time point is due to the diffusion time required for the drug to make it from the higher concentration in the vessel out to the distant sites of the tumor epithelium. This spatial concentration gradient induces the diffusive transport of the drug once it has passed out of the endothelial barrier. Measurement of the drug concentration at early times will always be confounded by this compartmentalization issue. However, the data plotted in Figs. 5(a) and 5(b) illustrate the different signals that would be measured from a small sampling region and a larger sampling region. In general, the mean values of these two distributions appear the same (p-values in Table 1), being 6.4 for the 15-min data and near 8.1 for the 3-h data. However, while the means of the distributions appear similar, the obvious difference is that the lowest and highest values of the distribution are lost in this latter case. The variances are significantly different, as shown by the f-test statistic and p-values shown in Table 1, illustrating that the distribution observed with pixel-level sampling is wider than the distribution observed when sampling is done over larger areas of tissue. Thus, sampling fluorescence from larger and larger regions has the affect of averaging the distribution function toward the mean value, and there is a loss of the lowest and highest parts of the histogram. It is not yet clear what implications these areas with very high and low drug levels may have on PDT treatment outcome. If measurement of the lowest and highest photosensitizer concentrations is important or useful for predicting tumor response, then sampling with smaller fibers and detectors will be important. However, sampling of many points on each tumor would then also be essential, similar to how Eppendorf oxygen electrode measurements of tumors require multiple points and multiple tracks to be used for a useful measurement of the oxygen distribution in a tumor.[30] It is possible that the mean value of photosensitizer concentration is all that is required, and then sampling with larger fibers should be sufficient.

We compare these microscopic data to the *in vivo* fiber measurements plotted in Fig. 6, and similar histograms are seen. The quantification of the mean and variance values of these distributions in Table 2 shows that the mean values between different animals can easily be different, and the variance values may or may not be different, depending on the physical characteristics of the drug diffusion and the sampling. The most important observation in this dataset is that the distributions are similar to those observed in Fig. 5 when image level sampling was completed, such that the ratio of the variance to the mean of the distribution is small. The cumulative data for any one animal show a histogram that has a variance that is in reasonable agreement with the microscopic data, yet appears as though the lowest and highest values of the histogram are not well represented [see Fig. 6(b)]. When data are pooled from several animals [Fig. 6(c)], then the full histogram appears more like a normal distribution, with values down to zero and up to the higher values. Thus, for any one animal, multiple sampling of the tumor is still useful, yet will not show the range of low and high values present in the tissue and the microscopic scale. This is a fundamental observation, that macroscopic sampling can likely never reveal the true range of concentrations existing in the tissue, because the distribution achieved has systematically averaged out the lowest and highest values. The only way to achieve the full distribution of values in the tissue is to sample at the tissue many times on a distance scale, which is smaller than the intercapillary spacing.

However, the choice of which size scale presents the "true" distribution is also a good question, and an extension of this study might also be to sample the tissue at the distance scale of the cell, or of subcellular organelles. These distance scales are also likely to present histogram distributions that are different than that observed on the intercapillary spacing distance scale. However, since the dominant factor in drug distribution is the diffusion or transport from the capillaries into the parenchyma, this study has focused on this latter scale, as compared to a macroscopic sampling scale of closer to 1 mm.

This study has not addressed the question of what the pertinent measurement of photosensitizer concentration is *in vivo*. It has been implied that the mean value of the concentration is the important parameter, and clearly photodynamic therapy effect scales with the drug dose in the tissue.[19,31–34] However, it is interesting to compare the photosensitizer histogram to the oxygen histogram observed in Eppendorf electrode studies.[35] In both radiation therapy and photodynamic therapy, there is good evidence to support the idea that the fraction of the tumor at the lowest oxygen tension is ultimately what limits the efficacy of therapy.[30,36–38] Thus, it is also conceivable that the fraction of the tumor that has low photosensitizer concentration is what limits the efficacy of photodynamic therapy. However, currently this is just a hypothesis, and is as yet untested. The main purpose of the present study was simply to understand what the measurement of fluorescence *in vivo* represents in terms of the true photosensitizer concentration in the tissue.

5 Conclusions

In conclusion, when fluorescence is measured *in vivo* the size of the region sampled appears to affect the measurement histogram of values, but does not strongly affect the mean value. As the region sampled is increased to larger than the typical intervascular distance, the histogram of values observed tends to lose the lowest and highest parts of the histogram. This is typically what can be observed with *in vivo* sampling of tissue with fiber optic probes. The macroscopic heterogeneity observed in many experimental tumors is an important issue for sampling of tumors, because if the measurement is taken from the exterior of the tumor, then the signal will be biased toward higher values than is representative of the full tumor. These effects on the sampled signal are likely difficult to avoid or correct for, but need to be well understood when interpreting *in vivo* data.

Further study of this effect could be carried out with fiber probes of varying diameter, and this work is ongoing presently. This study presents an initial interpretation of the size scales of heterogeneity observed in this experimental tumor system, using microscopy and a current working fiber probe system.

References

1. A. E. Profio and J. Sarnaik, "Fluorescence of HpD for tumor detection and dosimetry in photoradiation therapy," in *Porphyrin Localization and Treatment of Tumors*, J. G. D. Doiron, Ed., pp. 301–314, Alan R. Liss, New York (1984).
2. M. Panjehpour, R. E. Sneed, D. L. Frazier, M. A. Barnhill, S. F. O'Brien, W. Harb, and B. F. Overholt, "Quantification of phthalocyanine concentration in rat tissue using laser-induced fluorescence spectroscopy," *Lasers Surg. Med.* **13**(1), 23–30 (1993).
3. C. M. Gardner, S. L. Jacques, and A. J. Welch, "Fluorescence spectroscopy of tissue: recovery of intrinsic fluorescence from measured fluorescence," *Appl. Opt.* **35**(10), 1780–1792 (1996).
4. S. Andersson-Engels, C. Klinteberg, K. Svanberg, and S. Svanberg, "*In vivo* fluorescence imaging for tissue diagnostics," *Phys. Med. Biol.* **42**(5), 815–824 (1997).
5. B. W. Pogue, S. L. Gibbs, B. Chen, and M. Savellano, "Fluorescence imaging *in vivo*: raster scanned point-source imaging provides more accurate quantification than broad beam geometries," *Technol. Cancer Res. Treat.* **3**(1), 15–21 (2004).
6. C. C. Lee, B. W. Pogue, J. A. O'Hara, C. M. Wilmot, R. R. Strawbridge, G. C. Burke, and P. J. Hoopes, "Spatial heterogeneity and temporal kinetics of photosensitizer (AlPcS2) concentration in murine tumors RIF-1 and MTG-B," *Photochem. Photobiol. Sci.* **2**(2), 145–150 (2003).
7. Q. Peng, J. Moan, G. Farrants, H. E. Danielsen, and C. Rimington, "Localization of potent photosensitizers in human tumor LOX by means of laser scanning microscopy," *Cancer Lett.* **58**(1,2), 17–27 (1991).
8. N. S. Trivedi, H. W. Wang, A. L. Nieminen, N. L. Oleinick, and J. A. Izatt, "Quantitative analysis of Pc 4 localization in mouse lymphoma (LY-R) cells via double-label confocal fluorescence microscopy," *Photochem. Photobiol.* **71**(5), 634–639 (2000).
9. S. Iinuma, K. T. Schomacker, G. Wagnieres, M. Rajadhyaksha, M. Bamberg, T. Momma, and T. Hasan, "*In vivo* fluence rate and fractionation effects on tumor response and photobleaching: photodynamic therapy with two photosensitizers in an orthotopic rat tumor model," *Cancer Res.* **59**(24), 6164–6170 (1999).
10. S. Andersson-Engels and B. C. Wilson, "*In vivo* fluorescence in

clinical oncology: fundamentals and practical issues," *J. Cell Pharmacol* **3**, 48–61 (1991).

11. L. Lilge, C. O'Carroll and B. C. Wilson, "A solubilization technique for photosensitizer quantification in *ex vivo* tissue samples," *J. Photochem. Photobiol., B* **39**(3), 229–235 (1997).

12. G. J. Smith, "The effects of aggregation on the fluorescence and the triplet state yield of hematoporphyrin," *Photochem. Photobiol.* **41**, 123–126 (1985).

13. B. Aveline, T. Hasan, and R. W. Redmond, "Photophysical and photosensitizing properties of benzoporphyrin derivative monoacid ring A (BPD-MA)," *Photochem. Photobiol.* **59**(3), 328–335 (1994).

14. B. M. Aveline, T. Hasan, and R. W. Redmond, "The effects of aggregation, protein binding and cellular incorporation on the photophysical properties of benzoporphyrin derivative monoacid ring A (BPD-MA)," *J. Photochem. Photobiol., B* **30**(2,3), 161–169 (1995).

15. J. Moan, H. Anholt, and Q. Peng, "A transient reduction of the fluorescence of aluminium phthalocyanine tetrasulphonate in tumours during photodynamic therapy," *J. Photochem. Photobiol., B* **5**(1), 115–119 (1990).

16. B. M. Aveline, T. Hasan, and R. W. Redmond, "The effects of aggregation, protein binding and cellular incorporation on the photophysical properties of benzoporphyrin derivative monoacid ring A (BPD-MA)," *J. Photochem. Photobiol., B* **30**, 161–169 (1995).

17. B. M. Aveline and R. W. Redmond, "Can cellular phototoxicity be accurately predicted on the basis of sensitizer photophysics?" *Photochem. Photobiol.* **69**(3), 306–316 (1999).

18. B. M. Aveline, R. M. Sattler, and R. W. Redmond, "Environmental effects on cellular photosensitization: Correlation of phototoxicity mechanism with transient absorption spectroscopy measurements," *Photochem. Photobiol.* **68**(1), 50–61 (1998).

19. B. C. Wilson, M. S. Patterson, and L. Lilge, "Implicit and explicit dosimetry in photodynamic therapy: a new paradigm," *Lasers Med. Sci.* **12**, 182–199 (1997).

20. B. W. Pogue, and G. C. Burke, "Fiber optic bundle design for quantitative fluorescence measurement from tissue," *Appl. Opt.* **37**(31), 7429–7436 (1998).

21. C. C. Lee, B. W. Pogue, G. C. Burke, and P. J. Hoopes, "Comparison of photosensitizer (AlS2Pc) quantitation techniques: In situ fluorescence microsampling versus tissue chemical extraction," *Photochem. Photobiol.* **74**(3), 453–460 (2001).

22. B. W. Pogue and T. Hasan, "Fluorophore quantitation in tissue-simulating media with confocal detection," *IEEE J. Quantum Electron.* **2**(4), 959–964 (1996).

23. C. Sheng, B. W. Pogue, E. Wang, J. E. Hutchins, and P. J. Hoopes, "Assessment of photosensitizer dosimetry and tissue damage assay for photodynamic therapy in advanced-stage tumors," *Photochem. Photobiol.* **79**(6), 520–525 (2004).

24. A. M. Richter, B. Kelly, J. Chow, D. J. Liu, G. H. Towers, D. Dolphin, and J. G. Levy, "Preliminary studies on a more effective phototoxic agent than hematoporphyrin," *JNCI, J. Natl. Cancer Inst.* **79**(6), 1327–1332 (1987).

25. A. M. Richter, S. Cerruti-Sola, E. D. Sternberg, D. Dolphin, and J. G. Levy, "Biodistribution of tritiated benzoporphyrin derivative (3H-BPD-MA), a new potent photosensitizer, in normal and tumor-bearing mice," *J. Photochem. Photobiol., B* **5**(2), 231–244 (1990).

26. B. Chen, B. W. Pogue, I. A. Goodwin, J. A. O'Hara, C. M. Wilmot, J. E. Hutchins, P. J. Hoopes, and T. Hasan, "Blood flow dynamics after photodynamic therapy with verteporfin in the RIF-1 tumor," *Radiat. Res.* **160**(4), 452–459 (2003).

27. C. C. Lee, B. W. Pogue, G. C. Burke, and P. J. Hoopes, "Spatial heterogeneity and temporal kinetics of photosensitizer (AlPcS2) concentration in murine tumors RIF-1 and MTG-B," *Photochem. Photobiol. Sci.* **2**, 145–150 (2003).

28. X. Zhou, B. W. Pogue, B. Chen, and T. Hasan, "Analysis of effective molecular diffusion rates for verteporfin in subcutaneous versus orthotopic Dunning prostate tumors," *Photochem. Photobiol.* **79**(4), 323–331 (2004).

29. G. Helmlinger, F. Yuan, M. Dellian, and R. K. Jain, "Interstitial pH and pO2 gradients in solid tumors *in vivo*: high-resolution measurements reveal a lack of correlation," *Nat. Med.* **3**(2), 177–182 (1997).

30. M. R. Horsman, A. A. Khalil, D. W. Siemann, C. Grau, S. A. Hill, E. M. Lynch, D. J. Chaplin, and J. Overgaard, "Relationship between radiobiological hypoxia in tumors and electrode measurements of tumor oxygenation," *Int. J. Radiat. Oncol., Biol., Phys.* **29**(3), 439–442 (1994).

31. B. C. Wilson, M. S. Patterson, and D. M. Burns, "Effect of photosensitizer concentration in tissue on the penetration depth of photoactivating light," *Lasers Med. Sci.* **1**, 235–244 (1986).

32. C. J. Tralau, A. J. MacRobert, P. D. Coleridge-Smith, H. Barr, and S. G. Bown, "Photodynamic therapy with phthalocyanine sensitisation: quantitative studies in a transplantable rat fibrosarcoma," *Br. J. Cancer* **55**(4), 389–395 (1987).

33. M. S. Patterson, B. C. Wilson, and R. Graff, "*In vivo* tests of the concept of photodynamic threshold dose in normal rat liver photosensitized by aluminum chlorosulphonated phthalocyanine," *Photochem. Photobiol.* **51**(3), 343–349 (1990).

34. T. J. Farrell, B. C. Wilson, M. S. Patterson, and R. Chow, "The dependence of photodynamic threshold dose on treatment parameters in normal rat liver *in vivo*," *Proc. SPIE* **1426**, 146–155 (1991).

35. B. W. Pogue, K. D. Paulsen, J. A. O'Hara, C. M. Wilmot, and H. M. Swartz, "Estimation of oxygen distribution in RIF-1 tumors by diffusion model-based interpretation of pimonidazole hypoxia and eppendorf measurements," *Radiat. Res.* **155**(1 Pt 1), 15–25 (2001).

36. V. H. Fingar, T. J. Wieman, Y. J. Park, and B. W. Henderson, "Implications of a preexisting tumor hypoxic fraction on photodynamic therapy," *J. Surg. Res.* **53**(5), 524–528 (1992).

37. M. Hockel, C. Knoop, K. Schlenger, B. Vorndran, E. Baussmann, M. Mitze, P. G. Knapstein, and P. Vaupel, "Intratumoral pO2 predicts survival in advanced cancer of the uterine cervix," *Radiother. Oncol.* **26**(1), 45–50 (1993).

38. M. Hockel, K. Schlenger, B. Aral, M. Mitze, U. Schaffer, and P. Vaupel, "Association between tumor hypoxia and malignant progression in advanced cancer of the uterine cervix," *Cancer Res.* **56**(19), 4509–4515 (1996).